JMEPEG (2012) 21:287–297
DOI: 10.1007/s11665-011-9904-5

1059-9495/$19.00

Damaging Prediction of Difficult-to-Work Aluminum Alloys During Equal Channel Angular Pressing

Radu Comaneci, Luchian Zaharia, and Romeu Chelariu

(Submitted November 23, 2010; in revised form February 10, 2011)

Severe plastic deformation (SPD) is a well-established method in the recent years for grain refinement in metallic materials. Equal channel angular pressing (ECAP) is one of the most effective SPD techniques. Inherent failures of ECAP, consisting in billet damage, take place if not made a correct process design. In this article, the evolution of damaging for a difficult-to-work Al-Mg alloy during ECAP was investigated. A tridimensional finite element analysis was performed for four different die designs to study the influence of die geometry and process parameters on billet damaging. To validate modeling we used, load level and strain distribution were depicted. Experimental tests were performed to test the numerical prediction. The results show that cracking may be reduced or eliminated by inner fillet corner of the die channels. It was demonstrated that the predicted results were in good agreement with experimental data obtained for 5052 aluminum alloy. The direct effect of knowledge about load and damaging during ECAP is to prevent both tool and billet damage.

Keywords aluminum, damage, equal channel angular pressing, finite element analysis, severe plastic deformation

1. Introduction

Ultrafine grained (UFG) materials have been widely investigated due to their improved mechanical properties such as high strength and toughness (Ref 1, 2). As nanocrystalline or ultrafine grained metallic materials can show remarkable mechanical properties (Ref 3) as well as excellent superplasticity (Ref 4, 5), numerous studies involving these materials have been conducted during the last decade. Great interest in the manufacturing of bulk nanostructured materials (BNMs) has been raised, and many cases for widening the range of their application have been suggested.

According to Hall-Petch relationship (Ref 6), it is known that the strength (σ) and the hardness (HV) of the materials usually increase with the decrease of the average size of grains (d):

$$\sigma = \sigma_o + K \cdot d^{-1/2} \quad \text{(Eq 1)}$$

where σ_o is the intrinsic yield stress and K is a constant for the given material.

Severe plastic deformation (SPD) is a well-established method in the recent years for grain refinement in metals and alloys. Various techniques have been developed to obtain UFG materials (Ref 7). Among them, the equal channel angular pressing (ECAP) is one of the most effective processes. Originally developed and further enhanced by Segal (Ref 8), ECAP is a promising technique for producing UFG materials by large shear plastic deformation.

Figure 1 shows a schematic principle that outlines the important geometric factors of the ECAP process. In ECAP, a billet is pressed through a die that contains two equal cross-sectional channels.

In the vertical channel, the billet moves as a rigid body while all deformation is localized in the small area around the channel's meeting line (the bisecting plane). The metal is subjected to a simple shear strain under relative low pressure when compared to the traditional extrusion process (Ref 8).

Because the cross section of the billet remains the same during extrusion, the process can be repeated until the accumulated deformation reaches the imposed level. The billet removal involves a new development of ECAP procedure. The introduction of a new sample returns the ECAP process to the initial configuration which permits the next pressing cycle to follow. The new sample is inserted and pressed from the top and the previous sample moves to the right through horizontal channel of die. Four standard processing routes have been developed for grain refinement, depending on the sequences of twists around the billet long axis: route A, B_A, B_C, and C. Billet rotations after every pass are 0° in route A, alternating ±90° in route B_A, same sense 90° in route B_C, and 180° in route C.

Generally, geometries in ECAP are described as a channel angle of ϕ and an outer corner angle of ψ. Typical the ϕ angle is in range of 90…150°, but most used values are 90° and 120°. The ψ angle is defined by fillet radius of outer die channel and it results of calculations.

As the microstructures and the mechanical properties of the plastic-deformed materials are directly related to the degree of plastic deformation, the understanding of the strain and stress development is very important in a successful ECAP process design. The theoretical effective strain $\bar{\varepsilon}$ according to the die geometry is given in Eq 1, as formulated by Iwahashi et al. (Ref 9):

Radu Comaneci, Luchian Zaharia and **Romeu Chelariu,** Faculty of Materials Science and Engineering, Technical University "Gh. Asachi", D. Mangeron 61A, 700050 Iasi, Romania. Contact e-mails: comaneci@tuiasi.ro and amvric@yahoo.com.

$$\bar{\varepsilon} = \frac{1}{\sqrt{3}}\left[2\mathrm{ctg}\left(\frac{\phi}{2}+\frac{\psi}{2}\right) + \psi\mathrm{cosec}\left(\frac{\phi}{2}+\frac{\psi}{2}\right)\right] \quad \text{(Eq 1)}$$

where the significance of terms are revealed in Fig. 1. The introduction of an outer radius transition of the extrusion channels decreases both the strain (according to Eq 1) and load level by improving the material flow.

The fillets of both outer and inner channel edges decrease strain from the maximum 1.15 and 0.67 ($\phi = 90°$ and 120°, respectively) to the minimum 0.907 and 0.605, respectively. It becomes clear that fillet of the edge of die channels has an increased effect for the die with $\phi = 90°$.

From the grain refinement point of view, achieving a large amount of strain during ECAP is essentially. For this reason, many research activities in the direction of material flow (Ref 10, 11), deformation behavior (Ref 12), and strain distribution (Ref 13) have been undertaken. Influence of die geometry (Ref 14), material properties and process parameters (Ref 15, 16) on strain (in)homogeneity were mainly the subjects of numerous studies (Ref 17-19).

From the technological point of view, a successful SPD process requires to surpass two obstacles. First the load level (which directly affects the tool design, especially in large dimensions of the billet) and second an adequate formability of the material so that it can withstand high degrees of repeated deformation. Unfortunately, there are no criteria which ensure a guaranteed successful SPD of the material. Only a favorable stress distribution can decide the success of SPD.

Inherent failures of ECAP if not made a correct process design were reported. Among them, especially billets damages due to the cracking on their upper surfaces were found (Ref 20).

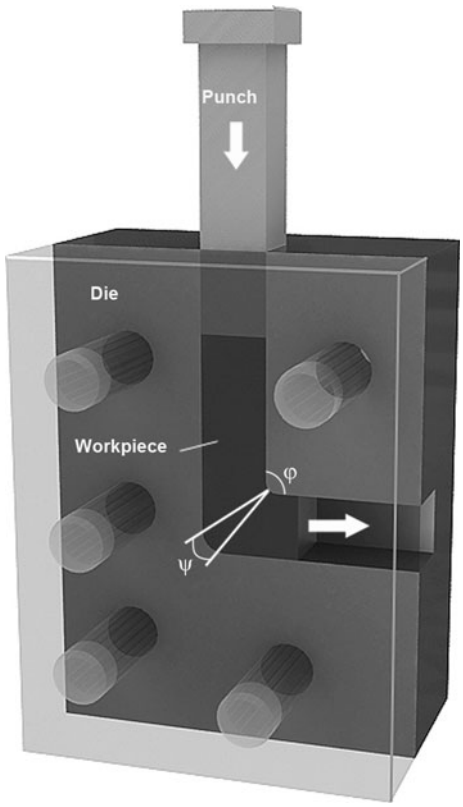

Fig. 1 Principle of ECAP and die geometry components

Concerning the billet damage during ECAP, two questions still remain standing: Which is precisely the influence of die geometry on the billet damage? and related to this, How one can avoid the failure of ECAP?

Damage generally relates to the likelihood of fracture in a part. The Cockcroft-Latham damage model has shown to be a good indicator of certain types of tensile ductile fracture (Ref 21, 22). According to this model, a damage factor (D_f) (which is a constant corresponding to a critical condition associated with fracture) is defined by the following relationship (Ref 21):

$$D_f = \int_0^{\bar{\varepsilon}_f} \sigma_T \, d\bar{\varepsilon} \quad \text{(Eq 2)}$$

where σ_T is the maximum principal tensile stress within the billet, $d\bar{\varepsilon}$ is the effective strain increment and the integral is evaluated from zero strain to the final effective strain, $\bar{\varepsilon}_f$.

The criterion was later normalized by incorporating the effective stress $\bar{\sigma}$ (Ref 23), to give normalized damage factor D_{fN}:

$$D_{fN} = \int_0^{\bar{\varepsilon}_f} \frac{\sigma_T}{\bar{\sigma}} d\bar{\varepsilon} \quad \text{(Eq 3)}$$

Using Eq 3, fracture occurs when D_{fN} reaches a critical value which depends upon the material and its processing history and which must be determined. This form of the Cockcroft-Latham relationship where the maximum principal tensile stress is normalized by the equivalent stress is generally considered to provide a reasonable prediction of the fracture of metals during ECAP processing (Ref 24) and therefore Eq 3 will be used in the following study.

Analytical studies have been carried out to investigate the deformation behavior of the billet during ECAP, such as strain analyses based on slip line theory and geometric considerations (Ref 25, 26).

Although these analytical methods surpass Eq 1, they do not directly account for the effect of strain hardening, much less its effect in combination with friction and/or die geometry. To overcome these limitations, finite element analyses (FEA) have been carried out (Ref 11, 17, 27, 28). Compared to analytical approaches, the FE method accounts more realistically for the material properties and boundary conditions and can serve as a guide for analytical models.

FEA results have been exposed and discussed in terms of effects of strain hardening, die geometry, and friction conditions especially on deformation behavior. For simplicity, many studies have used two-dimensional specific element codes (Ref 19, 27-30).

In this article, a tridimensional FEA is performed to analyze the ECAP process. The purpose of FEA is to evaluate the damage distribution during ECAP depending on die geometry and process parameters (such as friction conditions or speed of the punch) to successfully pursue the ECAP process. At the same time, to validate modeling we used, load level and strain distribution were depicted. Experimental tests were performed to test the numerical prediction. The direct effect of the knowledge of load and damaging during ECAP is to prevent both tool damage and cracking of billets. In this way, tool and process designs become more accurate with all the benefits for industrial implementation.

2. Experimental Materials and Procedures

2.1 Processing Al-Mg Alloy by ECAP

Wrought non-heat-treatable Al-Mg alloys are attractive candidates for different components due to their good weldability, moderate strength, but excellent corrosion resistance. Increasing strength by SPD without any supplementary alloying is a convenient way to rise up the potential of the material with maintaining all other mechanical properties.

In these conditions, there is considerable interest in using Al-Mg alloys for structural applications. But experiments have shown the successful pressing of Al-Mg alloys without billet cracking requires special consideration due to their limited workability by ECAP.

Al-Mg alloys, such as AA 5052, 5056 or 5083, were difficult to work by ECAP at room temperature. Usually, the extrusion operation becomes easier if pressing is conducted at elevated temperature (Ref 4, 5). In practice, however, an increase in the pressing temperature leads to an increase in as pressed grain size. In developing ECAP process at elevated temperature, the alloys were modified by adding extra amount of particle forming elements such as Zr (Ref 31) or Sc (Ref 32, 33) to prevent grain growth. But this method rises upping the processing price and operation becomes relatively expensive. Furthermore, the elaboration of these special alloys is not so simple. According to all these, it is preferable to conduct ECAP at room temperature with absence of any significant cracking in the billets.

A commercial available aluminum AA 5052 alloy with a composition in wt.% of 2.8%Mg-0.2%Cr and aluminum balance was used in this study. Specimens with dimensions of $10 \times 10 \times 60$ mm were machined from as-received alloy. A subsequent annealing at 723 K for 1 h was performed before ECAP. This results in the initial grain size of ≈100 μm.

The ECAP process was conducted at room temperature with a constant speed of 8.75 mm/s, using dies with $\phi = 90°$, Fig. 2.

All samples and inner walls of the dies channels were lubricated using zinc stearate. For the effect of die geometry on material behavior, the die corner angle ψ was varied as 0° and 28.7°, respectively, corresponding to an outer radius of 4 mm (R). An inner transition radius of 2 mm (r) was also considered. To confirm the modeling results of FEA, the evolution of working load versus punch displacement in one ECAP pass, with emphasis on the combined effects of material strain hardening (n), friction (μ), and die geometry (ϕ, ψ), was depicted.

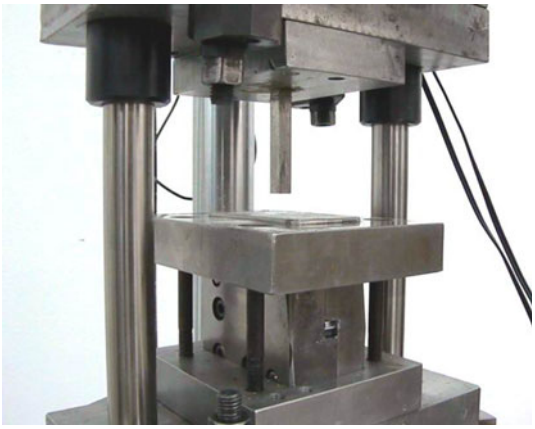

Fig. 2 Equipment used for ECAP processing

2.2 Finite Element Analysis

2.2.1 Conditions. In this study, a three-dimensional model was considered. Commercial finite element code DEFORM 3D was used to carried out the simulations.

The die and the punch were modeled with analytical rigid elements. All simulations were performed at room temperature, with the same speed of punch when compared with experimental speed.

The friction coefficient between inner die channels and billets was assumed to be 0.12. This value was established in an earlier work (Ref 34), and it has been considered by other authors (Ref 30).

The workpiece ($10 \times 10 \times 60$ mm) is considered a plastic body in whole deformation process. The workpiece was discretized in 8000 tetrahedral elements. According to Figueiredo et al. (Ref 23) a mesh of 8000 elements is sufficiently fine to reveal localized effects (this is equivalent to at least 36 elements across the width of the billet).

The tolerance, positioning of the workpiece and top/bottom die, convergence criteria, re-meshing conditions, and boundary conditions were specified before the execution of the simulation process:

- displacement and rotation in x, y, and z directions for all nodes in the die were arrested;
- top surface of the workpiece is in contact with the punch and takes load resulting in the moving of the workpiece.

Poisson's ratio 0.33 and Young's modulus 69 Gpa were assumed. The hardening behavior is considered isotropic and independent of strain rate at room temperature.

Stress-strain relationship was experimentally obtained by compression test. Samples with initial diameter of 12 and 15 mm height were pressed up to a reduction of 53%, which corresponds to a strain of 0.42. Experimental parameters (deformation speed and temperature) were identical to those used in finite element simulation. Flow stress evolves with strain according to σ (MPa) = $402.29 \cdot \varepsilon^{0.30}$ (see Fig. 3).

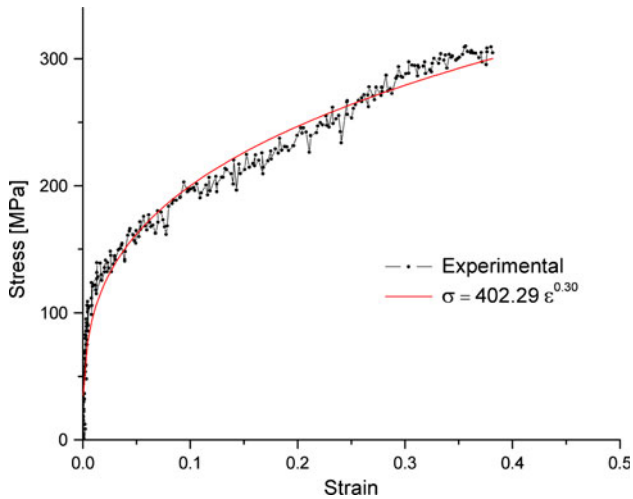

Fig. 3 Stress-strain curve of the material used in FE simulations

2.2.2 Die Design. For studying the overall deformation behavior of the workpiece, die geometry was involved. For a given channel angle (ϕ), the die geometry is described by outer and inner corner angles that mean by outer (R) and inner (r) corner radius, respectively. Together with friction conditions and strain hardening of material, die geometry determines the material behavior during ECAP.

Die geometry also has a significant influence both on the shear plane shape and its location and also determines the load-level and the stress distribution during ECAP. At the same time, the forming of so-called deformation dead zone and corner gap between material and outer corner of the die are depending of corners geometry (Ref 11).

The die considered for analysis corresponds to high strength hardened steel. The channel angle was 90° and outer corner radius of 4 mm (R) and inner corner radius of 2 mm (r) were considered.

Four design scenarios (symbolized 90_R_r) are analyzed by FEA to reveal the deformation behaviors and their relationship with the design configuration:

A. there is no arc transition, the channels are intersected at a sharp corner: R, r = 0 mm (90_0_0)
B. there is one arc transition at the inner side of the channels: R = 0 mm; r = 2 mm (90_0_2)
C. there is one arc transition at the outer side of the channels: R = 4 mm; r = 0 mm (90_4_0)
D. there are two arc transitions at both sides of the channels: R = 4 mm; r = 2 mm (90_4_2).

3. Results and Discussion

3.1 Working-Load Level and Strain Distribution. Validation of Modeling

3.1.1 Working-Load. For this research the deformation load is not so critical because of quite small billet dimensions. However, matching of simulates with experimental load results is important to validate the modeling we have used it. Also, the validity of Eq 1 can be confirmed by effective strain distribution within the material during ECAP.

Figure 4 shows load-displacement curve during the ECAP process of AA5052 alloy using a die with channel angle of $\phi = 90°$ and no significant outer/inner arc of curvature between channels, except only for a minor tolerance introduced during the machining operation, corresponding of $\psi \approx 3°$.

Four stages can be distinguished on load-displacement curve (Fig. 4).

In Stage I, the load increases rapidly with the ram displacement, reaching a maximum. This stage begins when the head of the billet first touches the bottom wall of the die channel at the outer corner and ends when the workpiece head bends over the corner (see Fig. 5).

In Stage II, the load decreases until the upper surface of the billet begins to touch the upper wall of the outlet channel.

In the next stage (Stage III), a slow increase in load marks the period from the moment the billet head touches the upper wall (end of Stage II) to the moment that sufficient contact is established between the upper surface of the billet head and the upper wall of the outlet channel. Load increases because of deformation in the billet head (see Fig. 5).

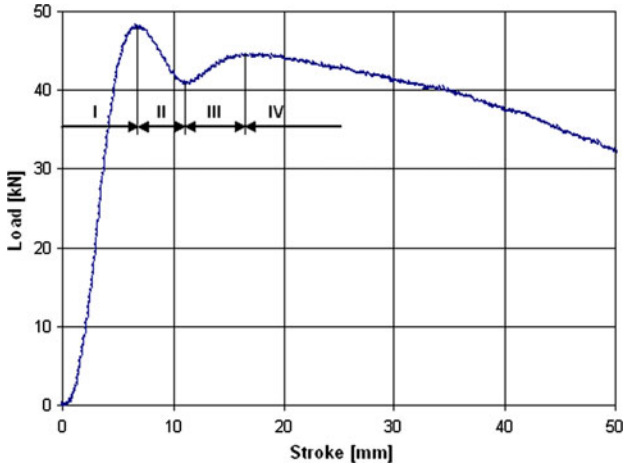

Fig. 4 Experimental load-displacement curve for one pass ECAP (AA 5052 alloy, ECAP 90_0_0)

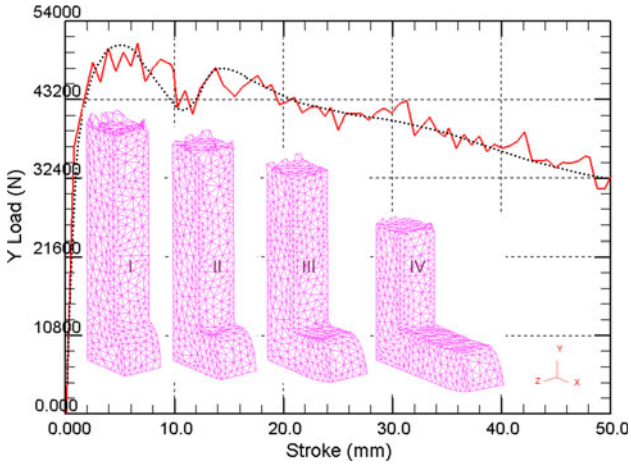

Fig. 5 Predicted load evolution for the first pass ECAP (90_0_0) of investigated alloy with emphasis of four different steps corresponding to stages I to IV

The load decreases gradually with the displacement in Stage IV. The decrease of load in the steady state region is related to the dependence of frictional forces on gap formation in the outlet channel. In general, the billet is in full contact with the die wall in the inlet channel, but only partially in contact with the wall in the outlet due to the formation of gaps. When the billet is pressed from the inlet channel to the outlet channel through the die corner, the contact area in the inlet channel decreases and in the meantime the length of the gap in the outlet channel grows until the head of the billet comes out of the outlet channel. As a result, the total contacting area between the billet and the die wall always decreases with the ram displacement, and so when we have real friction, the response is visible in the load versus displacement curve.

The magnitude of the maximum load is most interesting from the viewpoint of die designs. The present results show that the peak load is reached prior to achieving the steady state and it is higher than the steady state load. This is a normal feature for a strain hardenable material (Ref 29). For AA5052 alloy, the maximum ECAP working-load for the first pass is around 48 kN.

Figure 5 shows the predicted load evolution for the first pass of ECAP 90_0_0 scenario, where the four described stages can be identified. The maximum level of working-load and the general evolution are in good agreement with experimental results, confirming the validity of ECAP modeling. The dashed line highlights the evolution of load and helps to identify the four mentioned stages. Furthermore, different simulated steps of ECAP corresponding to the four stages were superimposed over graph.

As we can see from Fig. 6(c) (90_4_0 scenario) the influence of outer corner radius (R) is visible, determining a significant decrease in predicted working-load compared with the precedent case shown in Fig. 5. The curved die channel ($\Psi \neq 0$) allows for material to pass through it more easily, and load normally decreases. Additional inner corner radius (r) has not a comparable influence on the maximum load level (see Fig. 6b) (Ref 28). As we shall see the outer/inner corner radius determines significant influence on strain and stress distribution.

3.1.2 Strain Distribution. Theoretically, uniform strain in the entire sample can be achieved if the deformation follows simple shear perfectly. At the beginning of the extrusion the billet sticks on the die due to the friction and then starts flowing over that. The inability of the sample to flow along the sharp outer corner angle resembled in severely damaged mesh at the end of the extrusion. The surface of the mesh in contact with the die walls at the inner and outer sides of the samples did not deform unlike the mesh at the center of the sample. The non-uniform strain achieved in plastic deformation zone and the origin of inhomogeneous behavior is well-known (Ref 18). As the workpiece exits from the plastic deformation zone the strain distribution starts to stabilize and is no further variations in the strain. It is shown that at the middle of the total deformation step a steady state deformation behavior is found. Increase in the stroke length will increase this portion of the steady state region (Ref 29). For this work there is interest for strain distribution only in the steady state region, to confirm the validity of the modeling.

It can be found from the final geometries of the workpieces that the deformation histories are different for the head part and the tail part as well as the inner and outer parts in the steady state region of the workpiece. It is obviously that transient regions of the head and tail ends receive smaller amounts of strain. Figure 7 shows strain distribution as a color map for the first ECAP pass of investigated alloy.

For 90_0_0 and 90_0_2 cases, effective strains and their distributions are nearly identical: head and tail regions with low strain deformation, a highly deformed bottom region starting from the bottom corner due to less movement of the bottom surface of the material and finally a uniform deformation zone.

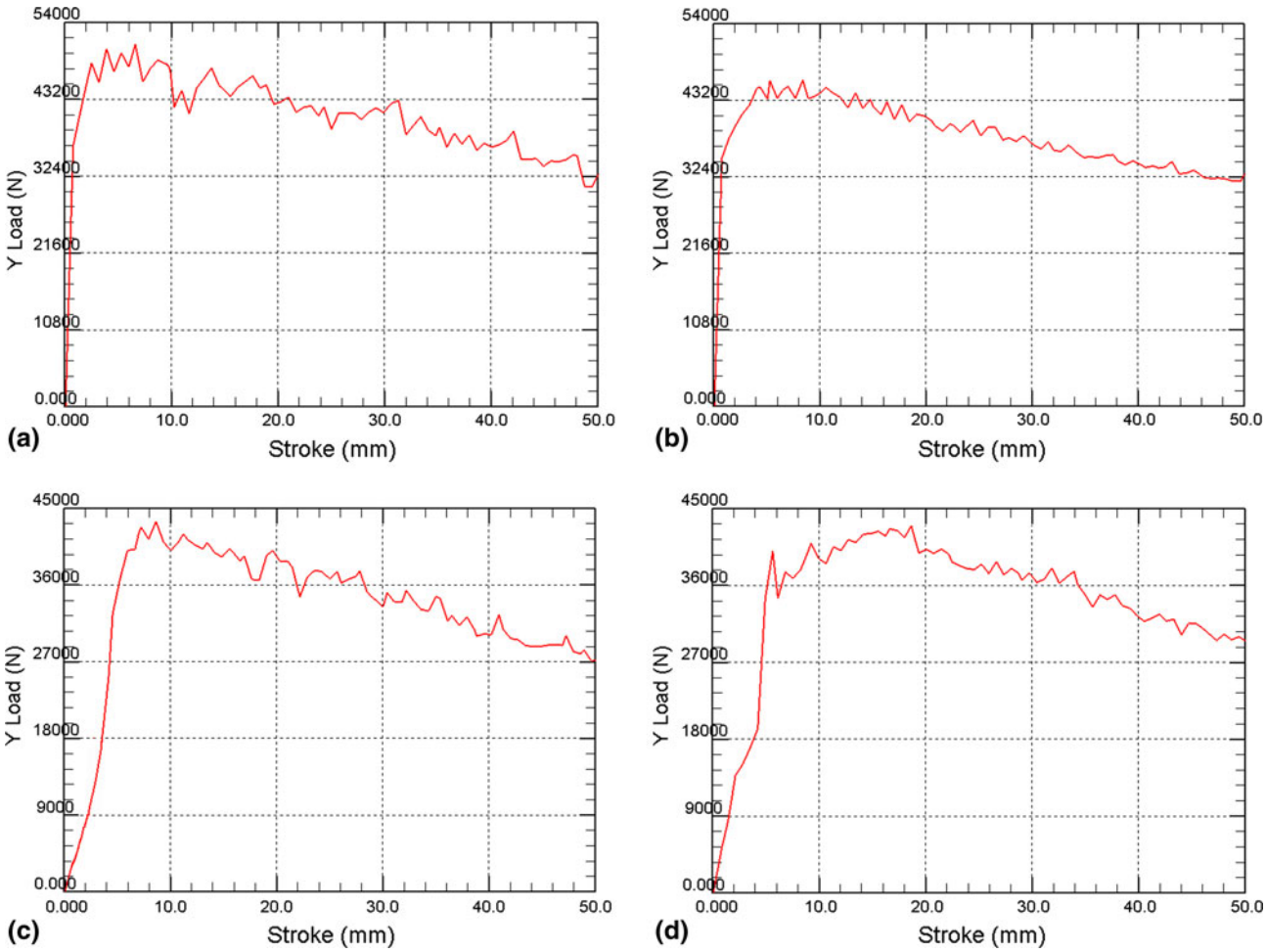

Fig. 6 Predicted load evolution for the first ECAP pass of investigated alloy (a) ECAP 90_0_0; (b) ECAP 90_0_2; (c) ECAP 90_4_0; (d) ECAP 90_4_2

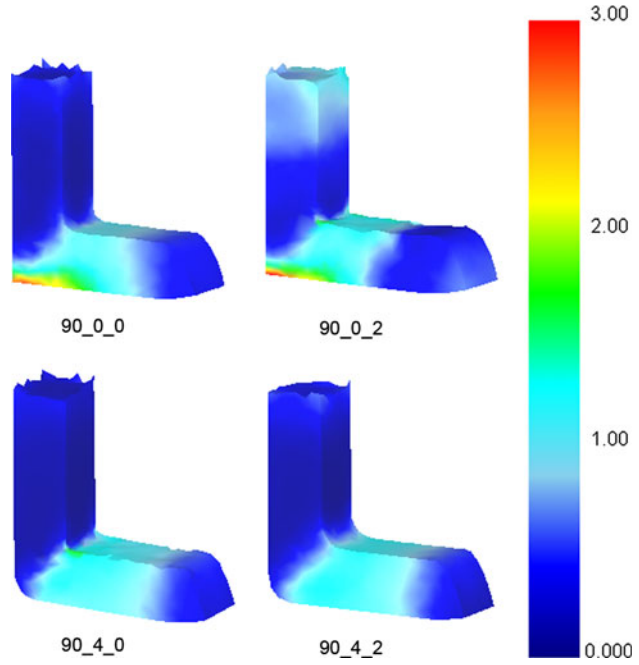

Fig. 7 Strain distribution for the first ECAP pass of investigated alloy (simulation)

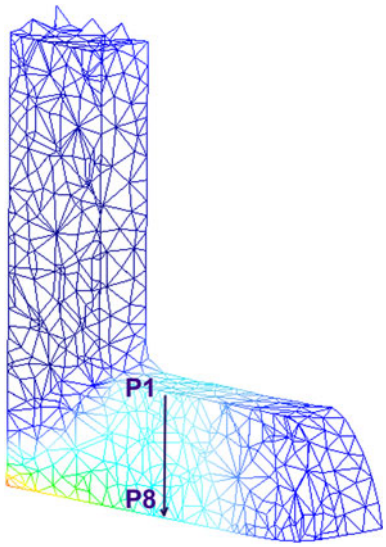

Fig. 8 The tracking points P1 to P8 defined in the longitudinal section of the steady state region of the billet

For 90_4_0 and 90_4_2 cases, the deformation zone is larger and the head end is a little bit shorter. Because of easier material flow around outer corner, no highly deformed zone at the bottom region was found. In both the cases, strain distributions were similar.

Because the color differences in the mentioned areas are unattachable, a few equidistant tracking points (P1, P2, … P8) are defined in longitudinal section of the workpiece across the width to estimate strain distribution after the material leaves the main deformation area corresponding to the bisecting plane of the die channels (Fig. 8).

The effective strain distributions along the path of the workpiece normal to the pressing direction in the steady state region for one pass ECAP are shown in Fig. 9(a) to (d).

For the sharp outer corner (90_0_0 and 90_0_2 scenario), the less movement of the bottom surface determines a more sheared bottom zone corner (corresponding to the point P8) and a top region less deformed (corresponding to the point P1). Contrary, for round outer corner (90_4_0 and 90_4_2 scenario) which induces rigid body motion flow without shear strain due to less constrain against the workpiece flow, the bottom region is less deformed.

Naturally and according to Eq 1, both outer and/or inner corner radius determine a decrease of the final effective strain. In all cases, final average strains from the steady state region are in good agreement with those given by Eq 1.

To provide a direct comparison between the simulations and the experimental results, the most inhomogeneous strain distribution occurring in 90_0_2 ECAP scenario was evaluated.

The method used to determine experimental strain distribution across the width of the processed billet was the known method of hardness-strain correlation for strain hardenable materials, based on Vickers microhardness tests (Ref 35-37). According to this method, the measured hardness is converted into the corresponding effective strain. This correlation is analytically expressed as a power function:

$$\mathrm{HV} = k(\bar{\varepsilon} + \varepsilon_o)^n \qquad \text{(Eq 4)}$$

where HV is the Vickers hardness, $\bar{\varepsilon}$ is the effective strain, ε_o is the offset strain, k and n are constants that designates the flow properties of the given material.

The effective strain-hardness curve of investigated alloy (Fig. 10) was obtained by compression tests carried out on cylindrical specimens with height-to diameter ratio $h/d = 1$, under the same conditions of temperature and speed as the ECAP. To avoid problems of inherent strain inhomogeneity, the hardness $\mathrm{HV}_{0.05}$ measurements were made around the center of the longitudinal section of the samples.

Thus, by means of the graph we have obtained an empirical law of correspondence between $\bar{\varepsilon}$ and $\mathrm{HV}(\bar{\varepsilon})$:

$$\mathrm{HV} = 79.65 \cdot (\bar{\varepsilon} + 0.105)^{0.225} \qquad \text{(Eq 5)}$$

Because the function $\mathrm{HV} = f(\bar{\varepsilon})$ is a bijection on its entire domain, a law of correspondence $\bar{\varepsilon} = f(\mathrm{HV})$ can be obtained as inverse function:

$$\bar{\varepsilon} = e^{\frac{1}{0.225}\cdot \ln \frac{\mathrm{HV}}{79.65}} - 0.105 \qquad \text{(Eq 6)}$$

To determine the experimental strain distribution ($\bar{\varepsilon}_{exp}$) for the highest found inhomogeneity, a billet of the investigated alloy was processed by ECAP in the 90_0_2 die, until the deformation process reached the stage corresponding to that indicated by the step tracer (solid line) from Fig. 9(b). The sample was then removed by disassembling the die and a longitudinal section obtained by electro-discharge machining (Fig. 11a) was prepared for microhardness tests (Fig. 11b). Five equidistant measurements ($\mathrm{HV}_{0.05}$) for each identified position P1 to P8 were performed to give corresponding average HV values.

To quantify the deformation inhomogeneity along the billet width a coefficient of variation of effective strain was calculated (Ref 30):

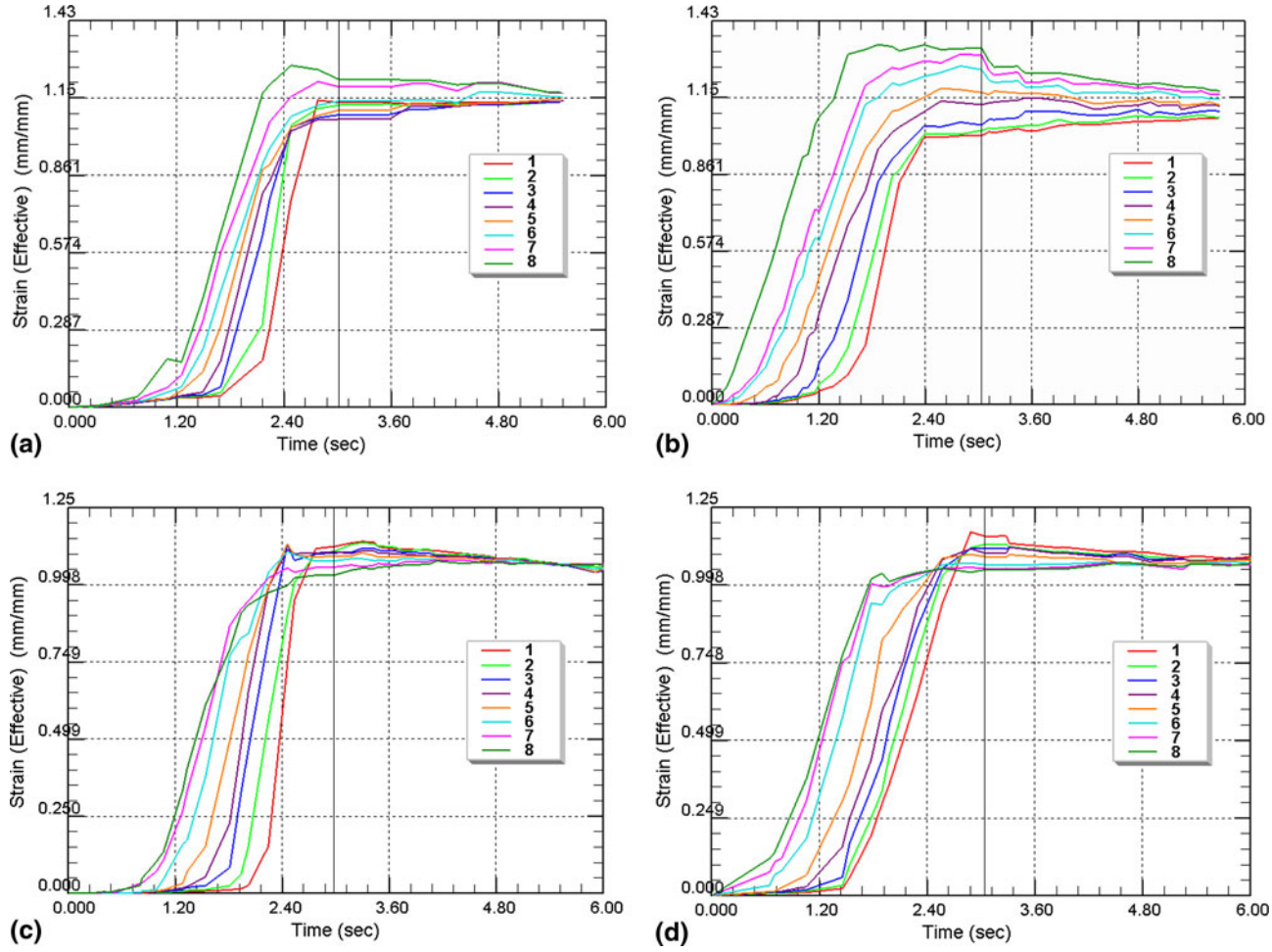

Fig. 9 Strain distribution in longitudinal section across the width of the workpiece (first pass ECAP of investigated alloy). Legend indicates the tracking points P1 to P8 (a) ECAP 90_0_0; (b) ECAP 90_0_2; (c) ECAP 90_4_0; (d) ECAP 90_4_2

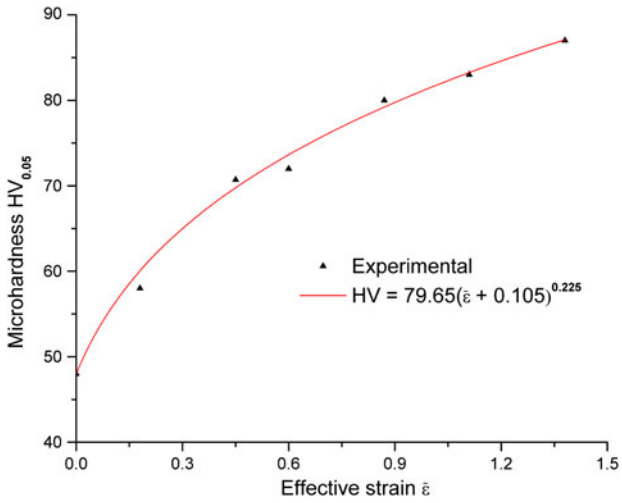

Fig. 10 Effective strain-hardness dependency of investigated alloy

$$CV_{\bar{\varepsilon}} = \frac{StDev\bar{\varepsilon}}{\bar{\varepsilon}_{ave}} (\%) \qquad \text{(Eq 7)}$$

where $StDev\bar{\varepsilon}$ and $\bar{\varepsilon}_{ave}$ are standard deviation and average of effective strain, respectively.

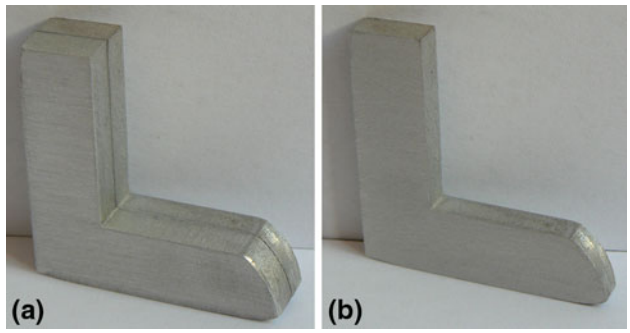

Fig. 11 Preparation of ECAP sample for microhardness measurements (a) ECAP sample cut in two halves by electro-discharge machining; (b) half-sample prepared for microhardness tests

The results are given in Table 1 in which experimental ($\bar{\varepsilon}_{exp}$) and simulated effective strain ($\bar{\varepsilon}_{sim}$ from Fig. 9b) were compared together with corresponding coefficients of variation.

As is noticeable the experimental and simulated results are in good agreement and strain inhomonogeneity ($CV_{\bar{\varepsilon}}$) closely match. Differences between experimental and simulated values corresponding to P1 and P8, respectively, are explained as different frictions—more on bottom surface (P8), less on top surface (P1). It thus validates the simulation.

Table 1 Experimental microhardness ($HV_{0.05}$), effective strains ($\bar{\varepsilon}_{exp}, \bar{\varepsilon}_{sim}$) and corresponding coefficients of variation ($CV\bar{\varepsilon}_{exp}, CV\bar{\varepsilon}_{sim}$) for 90_0_2 scenario

Position	$HV_{0.05}$	$\bar{\varepsilon}_{exp}$	$CV\bar{\varepsilon}_{exp}$, %	$\bar{\varepsilon}_{sim}$	$CV\bar{\varepsilon}_{sim}$, %
P1	80.9	0.97	11.30	1.01	9.82
P2	81.8	1.02		1.04	
P3	82.8	1.08		1.07	
P4	83.4	1.12		1.11	
P5	84.3	1.18		1.17	
P6	85.0	1.23		1.22	
P7	85.6	1.27		1.26	
P8	86.7	1.35		1.33	

Despite its presence, strain inhomogeneity is not a worrying fact, as long as it can be corrected by means of the next passes. For example, after four passes via route B_C a homogeneous strain distribution is achieved due to shearing along four crossed directions (Ref 13).

The microstructural changes have similar evolution. During first pass a substantial increase of the number of low-angle subgrains occurs (Ref 38) and strain hardening takes place accordingly to material flow properties. It results an inhomogeneous structure deformed along main shear direction. During second pass the fraction of high-angle grain boundaries increases and the deformation mechanism changes from dislocation slip to grain boundary sliding. Consequently, the material tends to a near-perfect-plastic behavior in compression (Ref 30).

Due to the interaction of the shearing planes with the deformation texture during next passes, the as-pressed microstructure evolves rapidly (usually four passes for aluminum alloys (Ref 39)) into an array of equiaxed grains separated by high-angle grain boundaries, resulting in a homogenous final structure. Because damaging is mainly related with both stress- and strain-state, microstructural changes cannot be directly quantified in a suitable manner for damaging prediction.

3.2 Prediction of Damaging During ECAP

3.2.1 Critical Damage. The normalized Cockcroft-Latham model assumes that fracture occurs in a ductile material when the damage factor (D_{fN}), reaches a certain value called critical damage factor (D_f^*) which depends upon the material and its process history. To determine the critical damage factor the alloy was tested in compression to failure to determine the maximum possible damage (accumulated damage). Then, the compression test was simulated by considering specimen having the same geometry as in real compression test and by characterizing the material behavior from the stress-strain curve recorded in compression test. To provide a direct correlation with the experiments, the simulation was stopped at the step where the reduction was similar to the maximum reduction in the experimental specimen at failure (Ref 30).

The stress and strain conditions for the compression test were then followed in the simulation thereby providing the critical damage factor which is in fact the accumulated damage at failure. The simulation performed in the mentioned conditions reveals that the critical damage factor for AA5052 was $D_f^* = 0.310$ (Fig. 12).

3.2.2 Damaging of Aluminum Alloy During ECAP. Using damage factor as defined in Eq 3, Fig. 13 shows damage distribution for the four scenarios. The highest level of damage

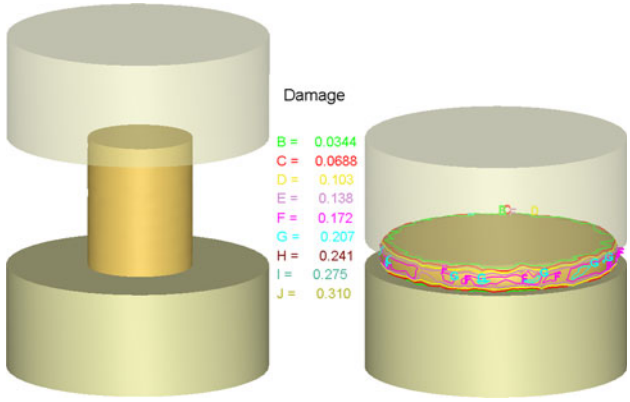

Fig. 12 The start simulation of the compression test and damage distribution in specimen at failure

(0.850) corresponds to 90_0_0 die. Outer fillet corner of the die channels (90_4_0 die) determines only a small decreasing of maximum damage (0.654). A significant change takes place for inner fillet corner of the die channels (90_0_2 die) when the level of damage down to the value of 0.230, due to increasing compressive deformation component.

In accord with failure condition ($D_{fN} > D_f^*$), the damage should clearly appears for the two cases A and C. Indeed, experimental data confirm this hypothesis. Figure 13 shows massive billets segmentation on upper surfaces of the billets for 90_0_0 and 90_4_0 scenario. For the case 90_4_2 only minor superficial cracks appear, which certifies the validity of the damaging prediction.

The nature of cracking on upper surfaces of the billet can be depicted from the stress distribution. High positive maximum principal stresses occur along the top surface of the billet in the exit channel immediately after the plane of channels intersection. Such an example can be seen in Fig. 14, and it is confirmed by other authors (Ref 30).

Summarizing, strain distribution is more related to outer corner radius while damage to inner corner radius. Outer corner radius facilitates material flow, but in turn determines a smaller shearing strain with all inconveniences on grain refinement (90_4_0 and 90_4_2 scenarios). Inner corner radius reduces damaging at the highest level of both shearing strain and inhomogeneity (90_0_2 scenario).

The described situation is synthesized by Fig. 15.

A balanced condition between strain inhomogeneity and damage is difficult to find because the damaging criterion is compulsory for each pass, no matter the situation. For grain refinement, an inhomogeneous shear strain (90_0_2) is preferable to a homogeneous strain obtained under less shearing condition (90_4_2 scenario) much more as the inhomogeneous strain can be corrected by next passes. Therefore, between smallest inhomogeneity with a high damage level and higher inhomogeneous strain with minimum damage level, we must choose the latter and otherwise this is a conclusion of this study.

4. Summary and Conclusions

FEA was performed to predict damaging of an aluminum-based alloy during ECAP. To estimate the damage, the

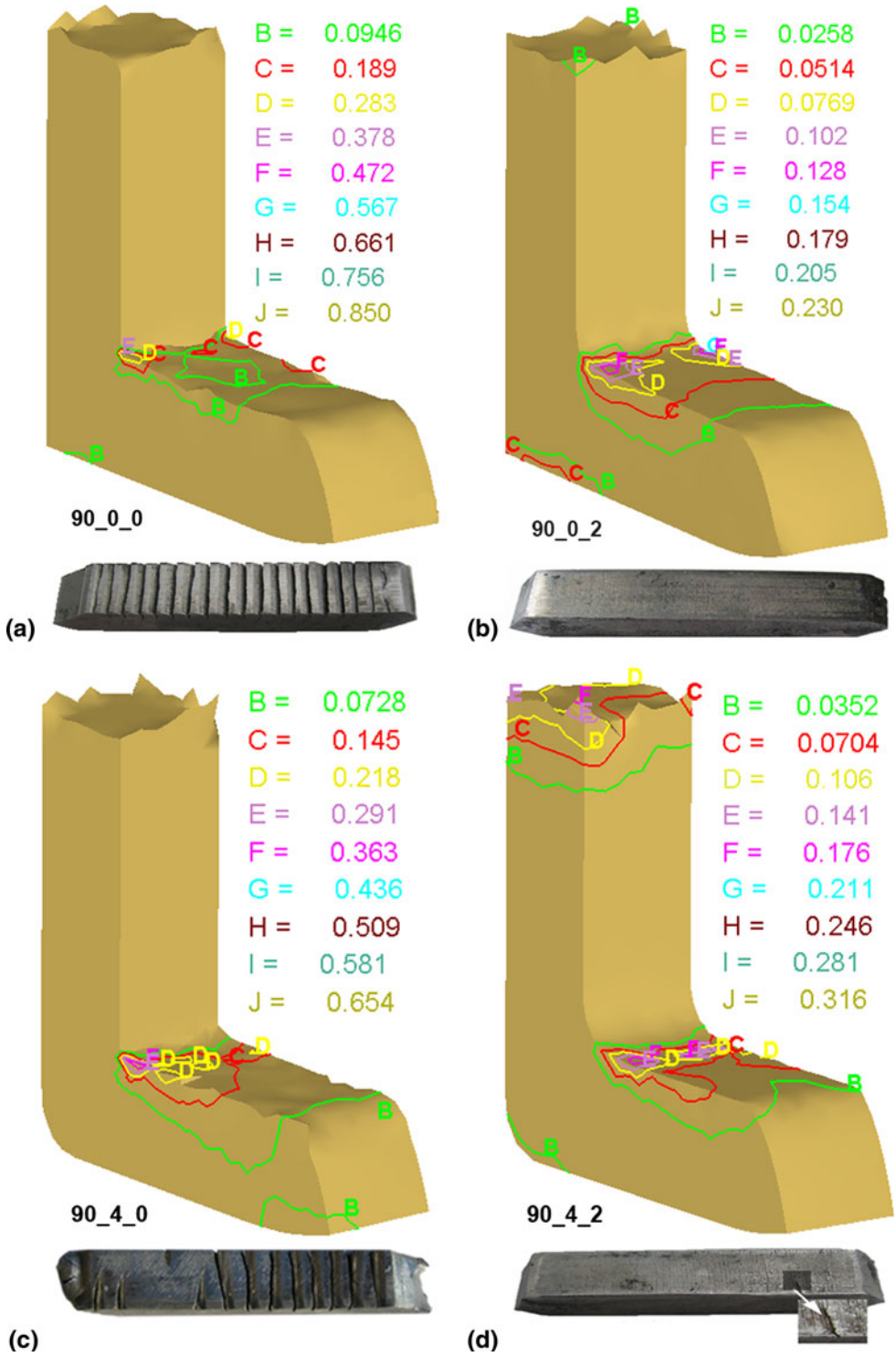

Fig. 13 Damage distribution and failure of specimens in ECAP scenarios (first pass, AA5052 alloy)

Cockroft-Latham model was used. The simulation used experimental data obtained from the compressive test of the material performed at room temperature.

The analysis shows that the die influences the damage during ECAP. Four design scenarios which included outer and/or inner corner radius of the die channels were analyzed. The die design with sharp outer corner and inner corner radius provides the minimum damage during ECAP.

FEM simulations suggest there will be crack formation in the material when the pressing reaches a damage factor higher than a critical value which was determined. The accumulation of high positive maximum stresses on the upper surface of the

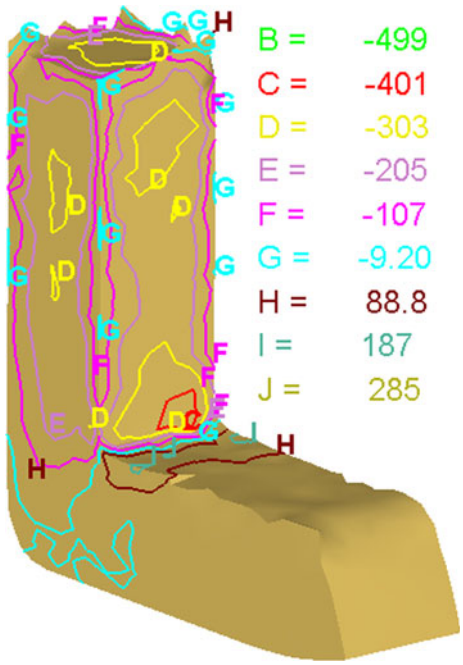

Fig. 14 Distribution of maximum principal stresses for AA5052, first pass ECAP 90_4_0 (simulation)

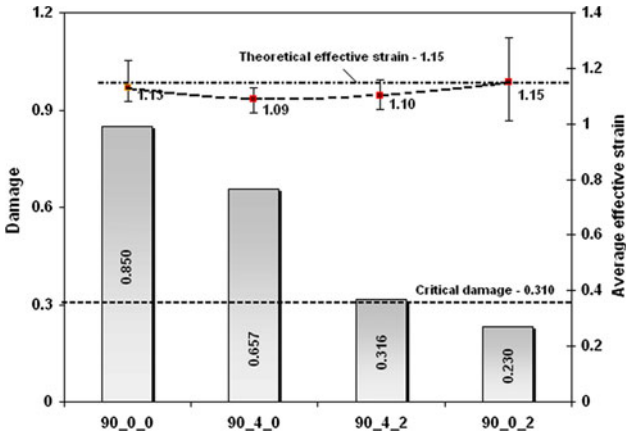

Fig. 15 Evolution of damage (column bars) and strain distribution for the four ECAP scenarios (simulation)

billets is the main cause of appearance of the cracks on the mentioned area.

References

1. P.J. Apps, C.P. Heason, and P.B. Prangnell, Ultrafine-Grain Structures produced by Severe Deformation Processing, *Mater. Sci. Forum*, 2004, **447–448**, p 423–428
2. B.Q. Han, E.J. Lavernia, and F.A. Mohamed, Mechanical Properties of Nanostructured Materials, *Rev. Adv. Mater. Sci.*, 2005, **9**, p 1–16
3. Y. Estrin, Effects of SPD: Mechanical Properties and Beyond, *Mater. Sci. Forum*, 2006, **503–504**, p 91–98
4. K.-T. Park, C.S. Lee, Y.S. Kim, and D.H. Shin, Superplastic Deformation of Ultrafine Grained Al Alloy Processed by ECAP and Post-Rolling, *Mater. Sci. Forum*, 2006, **503–504**, p 119–124
5. M. Noda, K. Funami, M. Hirohashi, and M. Kobayashi, Effect of Grain Size and Microstructure on Appearance of Low Temperature Superplasticity in Al-Mg Alloy, *Mater. Sci. Forum*, 2004, **447–448**, p 435–440
6. N. Tsuji, S. Okuno, T. Matsuura, Y. Koizumi, and Y. Minamino, Mechanical Properties as a Function of Grain Size in Ultrafine Grained Aluminum and Iron Fabricated by ARB and Annealing Process, *Mater. Sci. Forum*, 2003, **426–432**, p 2667–2772
7. A. Azushima, R. Kopp, A. Korhonen, D.Y. Yang, F. Micari, G.D. Lahoti, P. Groche, J. Yanagimoto, N. Tsuji, A. Rosochowski, and A. Yanagida, Severe Plastic Deformation (SPD) Processes for Metals, *CIRP Ann. Manuf. Technol.*, 2008, **57**, p 716–735
8. V.M. Segal, Materials Processing by Simple Shear, *Mater. Sci. Eng. A*, 1995, **197**, p 157–164
9. Y. Iwahashi, M. Furukawa, Z. Horita, M. Nemoto, and T.G. Langdon, Microstructural Characteristics of Ultrafine-Grained Aluminum Produced Using Equal-Channel Angular Pressing, *Metall. Mater. Trans.*, 1998, **29**(9), p 2245–2252
10. J.-Y. Suh, H.-S. Kim, J.-W. Park, and J.-Y. Chang, Finite Element Analysis of Material Flow in Equal Channel Angular Pressing, *Scripta Mater.*, 2001, **44**, p 677–681
11. H.S. Kim, M.H. Seo, and S.I. Hong, On the Die Corner Gap Formation in Equal Channel Angular Pressing, *Mater. Sci. Eng. A*, 2000, **291**, p 86–90
12. M. Reihanian, R. Ebrahimi, N. Tsuji, and M.M. Moshksar, Analysis of the Mechanical Properties and Deformation Behavior of Nanostructured Commercially Pure Al Processed by Equal Channel Angular Pressing ECAP, *Mater. Sci. Eng. A*, 2008, **473**, p 189–194
13. W.J. Kim, J.C. Namgung, and J.K. Kim, Analysis of Strain Uniformity During Multi-Pressing in Equal Channel Angular Extrusion, *Scripta Mater.*, 2005, **53**, p 293–298
14. S.C. Yoon, P. Quang, S.I. Hong, and H.S. Kim, Die Design for Homogeneous Plastic Deformation During Equal Channel Angular Pressing, *J. Mater. Process. Technol*, 2007, **187–188**, p 46–50
15. E. Cerri, P.P. De Marco, and P. Leo, FEM and Metallurgical Analysis of Modified 6082 Aluminium Alloys Processed by Multipass ECAP: Influence of Material Properties and Different Process Settings on Induced Plastic Strain, *J. Mater. Process. Technol.*, 2009, **209**, p 1550–1564
16. F. Djavanroodi and M. Ebrahimi, Effect of Die Channel Angle, Friction and Back Pressure in the Equal Channel Angular Pressing Using 3D Finite Element Simulation, *Mater. Sci. Eng. A*, 2010, **527**, p 1230–1235
17. V.P. Basavaraj, U. Chakkingal, and T.S. Prasanna Kumar, Study of Channel Angle Influence on Material Flow and Strain Inhomogeneity in Equal Channel Angular Pressing Using 3D Finite Element Simulation, *J. Mater. Process. Technol.*, 2009, **209**, p 89–95
18. W. Wei, A.V. Nagasekhar, G. Chen, Y. Tick-Hon, and K.X. Wei, Origin of Inhomogeneous Behavior During Equal Channel Angular Pressing, *Scripta Mater.*, 2006, **54**, p 1865–1869
19. A.V. Nagasekhar, Y. Tick-Hon, and H.P. Seow, Deformation Behavior and Strain Homogeneity in Equal Channel Angular Extrusion/Pressing, *J. Mater. Process. Technol.*, 2007, **192–193**, p 449–452
20. M. Vedani, P. Bassani, M. Cabibbo, and E. Evanghelista, Experimental Aspects Related to Equal Channel Angular Pressing of a Commercial AA6082 Alloy, *Metall. Sci. Technol.*, 2003, **21**(2), p 3–10
21. M.G. Cockcroft and D.J. Latham, Ductility and the Workability of Metals, *J. Inst. Met.*, 1968, **96**, p 33–39
22. M.A. Shabara, A.A. El-Domiaty, and A. Kandil, Validity Assessment of Ductile Fracture Criteria in Cold Forming, *J. Mater. Eng. Perform.*, 1996, **5**(4), p 478–488
23. R.B. Figueiredo, T.G. Langdon, and P.R. Cetlin, The Processing of Difficult-to-Work Alloys by ECAP with an Emphasis on Magnesium Alloys, *Acta Mater.*, 2007, **55**, p 4769–4779
24. S.C. Yoon, C.H. Bok, M.H. Seo, T.-S. Kim, and H.S. Kim, Comparison in Deformation and Fracture Behavior of Magnesium During Equal Channel Angular Pressing by Experimental and Numerical Methods, *Mater. Trans.*, 2008, **49**, p 963–966
25. V.M. Segal, Slip Line Solutions, Deformation Mode and Loading History During Equal Channel Angular Extrusion, *Mater. Sci. Eng. A*, 2003, **345**, p 36–46
26. A.R. Eivani and A. Kamiri Taheri, The Effect of Dead Metal Zone Formation and Extrusion Force During Equal Channel Angular Extrusion, *Comput. Mater. Sci.*, 2008, **42**, p 14–20
27. A.V. Nagasekhar and Yip Tick-Hon, Optimal Tool Angles for Equal Channel Angular Extrusion of Strain Hardening Materials by Finite Element Analysis, *Comput. Mater. Sci.*, 2004, **30**, p 489–495

28. S.C. Yoon and H.S. Kim, Finite Element Analysis of the Effect of the Inner Corner Angle in Equal Channel Angular Pressing, *Mater. Sci. Eng. A*, 2008, **490**, p 438–444
29. S. Li, M.A.M. Bourke, I.J. Beyerlein, D.J. Alexander, and B. Clausen, Finite Element Analysis of the Plastic Deformation Zone and Working Load in Equal Channel Angular Extrusion, *Mater. Sci. Eng. A*, 2004, **382**, p 217–236
30. R.B. Figueiredo, P.R. Cetlin, and T.G. Langdon, The Evolution of Damage in Perfect-Plastic and Strain Hardening Materials Processed by Equal-Channel Angular Pressing, *Mater. Sci. Eng. A*, 2009, **518**, p 124–131
31. R.K. Islamgaliev, N.F. Yunusova, and R.Z. Valiev, The Influence of the SPD Temperature on Superplasticity of Aluminium Alloys, *Mater. Sci. Forum*, 2006, **503–504**, p 585–590
32. F. Musin, R. Kaibyshev, Y. Motohashi, and G. Itoh, Superplastic Behaviour and Microstructure Evolution in a Commercial Ultra-Fine Grained Al-Mg-Sc Alloy, *Mater. Sci. Forum*, 2004, **447–448**, p 417–422
33. K.-T. Park, C.S. Lee, and D.H. Shin, Superplastic Behavior of As-Equal Channel Angular Pressed 5083 Al and 5083 Al-0.2 Sc Alloys, *Mater. Sci. Forum*, 2005, **475–479**, p 2937–2940
34. C. Chirita, R. Comaneci, L. Zaharia, and A.C. Hanganu, Technological Aspects Concerning Severe Plastic Deformation by Equal Channel Angular Pressing, Annals of DAAAM for 2007, *Proceedings of the 18th International DAAAM Symposium*, B. Katalinic, Ed., October 24-27, 2007 (Zadar, Croatia), DAAAM International, Vienna, 2007, p 139–140
35. J. Petruska and L. Janícek, On the Evaluation of Strain Inhomogeneity by Hardness Measurement of Formed Products, *J. Mater. Process. Technol.*, 2003, **143–144**, p 300–305
36. F.O. Sonmez and A. Demir, Analytical Relations Between Hardness and Strain for Cold Formed Parts, *J. Mater. Process. Technol.*, 2007, **186**(1–3), p 163–173
37. D. Iordachescu, M. Iordachescu, J. Planas, J.L. Ocana, and M. Blasco, Strain-hardness correlation in aluminium butt cold welded joints. *Weld World* 2008, **52**(Spec Iss), p 759–763
38. M. Furukawa, M. Nemoto, and Z. Horita, Processing of Metals by Equal-Channel Angular Pressing, *J. Mater. Sci.*, 2001, **36**, p 2835–2843
39. Y.T. Zhu and T.C. Lowe, Observations and Issues on Mechanisms of Grain Refinement during ECAP Process, *Mater. Sci. Eng. A*, 2000, **291**, p 46–53